Research Article

Altermagnetic Spectral Splitting without Net Magnetization: Exact Symmetry and Interaction Effects in a Two-Sublattice Hubbard Model

Agum Abdillah
Independent Researcher
North Masbagik, East Lombok, West Nusa Tenggara, Indonesia
itsagummm@atomicmail.io

Abstract. We formulate an exact constraint on the interacting one-particle Green function of a compensated two-sublattice model whose symmetry combines a quarter-turn in momentum space with a spin and sublattice transformation. For an equilibrium density matrix invariant under this operation, the full Green matrix obeys a covariance relation that exchanges the spin-resolved sublattice blocks at rotated momenta. The traced spectral functions consequently satisfy $A_\uparrow(\mathbf{k}, \omega) = A_\downarrow(R\mathbf{k}, \omega)$, while the Brillouin-zone-integrated uniform spin polarization vanishes. The identity is independent of perturbative order and does not assume quasiparticles; it constrains, but does not by itself require, a nonzero momentum-resolved splitting. We realize the symmetry in a two-sublattice Hubbard model with a compensated staggered source, derive its analytic noninteracting spectrum and first-order Hartree renormalization, and test the interacting spectral structure by Lanczos exact diagonalization on an eight-site cluster. We further calculate the full nonlocal second-order Hubbard self-energy in real space, express its retarded continuation as a three-spectral-function convolution, and verify its symmetry covariance and causal sign numerically. The results establish a symmetry-controlled route to interaction-renormalized altermagnetic spectral splitting in a compensated, source-pinned state.

Keywords: altermagnetism; interacting Green function; spectral function; Hubbard model; compensated magnetism; self-energy.

1. Introduction

A defining feature of altermagnetic band structures is the coexistence of zero net magnetic moment with a spin splitting that changes sign under selected transformations of crystal momentum. This combination distinguishes altermagnetic order from both a conventional ferromagnet, where spin polarization is tied to a nonzero uniform moment, and a conventional compensated antiferromagnet, where the relevant symmetries can protect spin degeneracy. The nonrelativistic spin-group formulation made this distinction precise and identified the role of crystal operations relating opposite-spin sublattices [1, 2]. Subsequent symmetry classifications have clarified the range of spin-space-group realizations and their relation to magnetic crystal structures [3].

The band-level statement leaves a many-body question. When the electrons interact, the object carrying the spectral information is no longer a static Bloch Hamiltonian but the full matrix Green function. Its self-energy can be momentum-, frequency-, orbital-, and spin-dependent. A symmetry statement formulated only for bare bands does not display how these structures transform, nor does it make explicit which part of the spin-resolved spectrum is constrained to cancel in a Brillouin-zone integral. The appropriate starting point is therefore the covariance of the interacting Green matrix itself.

Here we consider a minimal two-sublattice Hubbard model with a staggered source that selects a compensated domain while preserving a combined quarter-turn and spin-sublattice symmetry. The source is not used as a proxy for a spontaneous ordering mechanism. It provides a symmetry-invariant background in which the exact spectral constraint, its interaction corrections, and its finite-cluster realization can be studied without ambiguity about the chosen domain. The central result is an exact covariance identity for the thermal Green function. It implies an antisymmetry of the traced spin-resolved spectral contrast under a fourfold momentum rotation and hence zero integrated uniform spin polarization. The identity is valid for arbitrary Hubbard interaction strength whenever the equilibrium state shares the combined symmetry.

We then make the constraint concrete. The noninteracting spectrum has an analytic momentum-dependent splitting. At first order in the Hubbard interaction, the Hartree term renormalizes the staggered exchange without spoiling the combined symmetry. An eight-site Lanczos calculation tests the spectral peaks and weights over a range of interactions, while a separate weak-coupling calculation evaluates the full nonlocal self-energy through order U^2. The exact-diagonalization and perturbative calculations address complementary regimes and are not treated as a same-size numerical comparison.

The paper is organized as follows. Section 2 defines the model and its symmetry. Section 3 proves the Green-function identity and the compensation relation. Section 4

analyzes the spectral splitting and the first-order interaction correction. Section 5 presents the finite-cluster benchmark. Section 6 gives the second-order dynamical self-energy and its numerical checks. The final section identifies the content and the precise scope of the results.

2. Two-sublattice Hubbard model and combined symmetry

Let $a = A, B$ label the two sites in a unit cell and let $\sigma = \uparrow, \downarrow$ denote spin along the z axis. We use the Bloch spinor

$$\Psi_{\mathbf{k}} = (c_{\mathbf{k}A\uparrow}, c_{\mathbf{k}B\uparrow}, c_{\mathbf{k}A\downarrow}, c_{\mathbf{k}B\downarrow})^T, \tag{1}$$

with Pauli matrices σ_i and τ_i acting in spin and sublattice space, respectively. The Hamiltonian is

$$H = \sum_{\mathbf{k}} \Psi^\dagger_{\mathbf{k}} h(\mathbf{k}) \Psi_{\mathbf{k}} + U \sum_{\mathbf{R},a} n_{\mathbf{R}a\uparrow} n_{\mathbf{R}a\downarrow}, \tag{2}$$

where

$$h(\mathbf{k}) = \epsilon_{\mathbf{k}} I_4 + I_\sigma \otimes (t_1 \tau_x + g_{\mathbf{k}} \tau_z) - \Delta \sigma_z \otimes \tau_z, \tag{3}$$

with

$$\epsilon_{\mathbf{k}} = -2t_0(\cos k_x + \cos k_y), \qquad g_{\mathbf{k}} = -2t_z(\cos k_x - \cos k_y). \tag{4}$$

The parameter t_1 is the intracell hopping, t_z is the anisotropic same-sublattice hopping, U is the onsite Hubbard repulsion, and Δ is a staggered exchange source. The latter couples with opposite signs to the two sublattices. It selects a compensated domain, rather than generating a net ferromagnetic moment. Unless stated otherwise, the calculations use $t_0 = 0$, $t_1 = 1$, and $t_z = 1/4$.

Consider the momentum-space rotation

$$R(k_x, k_y) = (-k_y, k_x), \tag{5}$$

for which $\epsilon_{R\mathbf{k}} = \epsilon_{\mathbf{k}}$ and $g_{R\mathbf{k}} = -g_{\mathbf{k}}$. Define

$$W = i\sigma_x \otimes \tau_x. \tag{6}$$

The internal transformation acts as

$$W(I \otimes \tau_x)W^\dagger = I \otimes \tau_x, \quad W(I \otimes \tau_z)W^\dagger = -I \otimes \tau_z, \tag{7}$$

while

$$W(\sigma_z \otimes \tau_z)W^\dagger = \sigma_z \otimes \tau_z. \tag{8}$$

It follows that

$$W h(\mathbf{k}) W^\dagger = h(R\mathbf{k}). \tag{9}$$

The Hubbard interaction is invariant under the corresponding site permutation and global spin rotation: it is an onsite spin scalar and is unchanged by relabelling the two sublattices. Thus the full Hamiltonian has a unitary combined symmetry $\mathcal{S}$ represented in the Bloch basis by

$$\mathcal{S}\Psi_{\mathbf{k}}\mathcal{S}^{-1} = W\Psi_{R\mathbf{k}}, \qquad [H, \mathcal{S}] = 0. \tag{10}$$

The operation reverses uniform S^z and exchanges the two sublattices. The product $\sigma_z\tau_z$ is invariant, so the staggered source in equation (3) does not break $\mathcal{S}$.

3. Exact covariance of the interacting Green function

Let ρ be an equilibrium density matrix satisfying

$$\mathcal{S}\rho\mathcal{S}^{-1} = \rho. \tag{11}$$

For example, the grand-canonical density matrix $\rho = Z^{-1}\exp[-\beta(H - \mu N)]$ has this property because both H and the total number operator N are invariant. Define the imaginary-time Green matrix

$$G_{ab}(\mathbf{k}, \tau) = -\operatorname{Tr}\Big[\rho\, T_\tau \Psi_{\mathbf{k},a}(\tau)\Psi^\dagger_{\mathbf{k},b}(0)\Big]. \tag{12}$$

Theorem 3.1 (Exact interacting Green-function covariance)**.** *If the Hamiltonian and equilibrium density matrix are invariant under the combined operation in equation (10), then the full interacting Green matrix satisfies*

$$G(\mathbf{k}, z) = W G(R\mathbf{k}, z) W^\dagger \tag{13}$$

for every complex frequency z in its domain of analyticity.

Proof. Because $[H, \mathcal{S}] = 0$, the symmetry action commutes with imaginary-time evolution. Inserting $\mathcal{S}^{-1}\mathcal{S}$ into the trace and using equation (11) gives

$$\begin{aligned} G(\mathbf{k}, \tau) &= -\operatorname{Tr}\Big[\rho\, T_\tau (\mathcal{S}\Psi_{\mathbf{k}}(\tau)\mathcal{S}^{-1})(\mathcal{S}\Psi^\dagger_{\mathbf{k}}(0)\mathcal{S}^{-1})\Big] \\ &= W\left[-\operatorname{Tr}\Big(\rho\, T_\tau \Psi_{R\mathbf{k}}(\tau)\Psi^\dagger_{R\mathbf{k}}(0)\Big)\right] W^\dagger \\ &= W G(R\mathbf{k}, \tau) W^\dagger. \end{aligned} \tag{14}$$

Fourier transformation in imaginary time yields the same relation for Matsubara frequencies. Analytic continuation establishes it throughout the common analytic domain. □

The theorem is not a perturbative statement. It applies to the exact Green function at arbitrary U, including all contributions to the self-energy, provided the equilibrium state is invariant under $\mathcal{S}$. In the collinear model without spin-orbit coupling, the Green matrix is block diagonal in spin. Equation (13) then gives

$$G_{\uparrow\uparrow}(\mathbf{k}, z) = \tau_x G_{\downarrow\downarrow}(R\mathbf{k}, z)\tau_x, \tag{15}$$

and the corresponding relation with $\uparrow$ and $\downarrow$ interchanged.

Define the sublattice-traced spectral function for each spin by

$$A_s(\mathbf{k}, \omega) = -\frac{1}{\pi} \operatorname{Im} \operatorname{Tr}_\tau G^R_{ss}(\mathbf{k}, \omega), \tag{16}$$

and the spin-resolved contrast by $D(\mathbf{k}, \omega) = A_\uparrow(\mathbf{k}, \omega) - A_\downarrow(\mathbf{k}, \omega)$. Taking the sublattice trace of equation (15) removes the unitary conjugation and gives

$$A_\uparrow(\mathbf{k}, \omega) = A_\downarrow(R\mathbf{k}, \omega), \qquad D(R\mathbf{k}, \omega) = -D(\mathbf{k}, \omega). \tag{17}$$

Since R preserves the Brillouin-zone measure,

$$\int_{\mathrm{BZ}} \frac{\mathrm{d}^2 k}{(2\pi)^2} D(\mathbf{k}, \omega) = 0 \tag{18}$$

for every frequency. The uniform spin polarization per unit cell is therefore

$$M_z = \frac{1}{2}\sum_s s \int_{\mathrm{BZ}} \frac{\mathrm{d}^2k}{(2\pi)^2} \int_{-\infty}^{\infty} \mathrm{d}\omega\, f(\omega) A_s(\mathbf{k},\omega) = 0, \tag{19}$$

where $s = +1$ for $\uparrow$ and $s = -1$ for $\downarrow$. The vanishing also follows directly because $\mathcal{S}$ reverses uniform S^z while leaving the equilibrium state invariant.

Remark 3.2 (What the symmetry does and does not determine)**.** Equation (17) constrains the relation between opposite-spin spectra at rotated momenta. It does not require $D(\mathbf{k},\omega)$ to be nonzero at a given momentum. A nonzero local contrast must follow from the Hamiltonian and the chosen compensated state. In a model with additional orbitals, the sewing matrix may depend on momentum; the full matrix covariance should then be retained until the appropriate orbital trace or projection is specified. With spin-orbit coupling, spin-projected spectral measures must be defined using the actual spin-orbital representation.

4. Analytic spectral splitting and the first-order interaction correction

For $U = 0$, spin $s = \pm 1$ has the two-band Hamiltonian

$$h_s(\mathbf{k}) = \epsilon_{\mathbf{k}} I_2 + t_1 \tau_x + (g_{\mathbf{k}} - s\Delta)\tau_z. \tag{20}$$

Its energies are

$$E_{s,\lambda}(\mathbf{k}) = \epsilon_{\mathbf{k}} + \lambda\sqrt{t_1^2 + (g_{\mathbf{k}} - s\Delta)^2}, \qquad \lambda = \pm 1. \tag{21}$$

At a generic momentum for which $g_{\mathbf{k}}\Delta \neq 0$, the spin-resolved poles are distinct. For the upper band,

$$\begin{aligned}\delta E_+(\mathbf{k}) &= E_{\uparrow,+}(\mathbf{k}) - E_{\downarrow,+}(\mathbf{k}) \\ &= -\frac{4 g_{\mathbf{k}}\Delta}{\sqrt{t_1^2 + (g_{\mathbf{k}} - \Delta)^2} + \sqrt{t_1^2 + (g_{\mathbf{k}} + \Delta)^2}}.\end{aligned} \tag{22}$$

The splitting changes sign under R and vanishes on the lines where $g_{\mathbf{k}} = 0$. The lower-band splitting has the opposite sign. These relations realize the exact spectral constraint in a transparent one-particle limit; the spin splitting is not uniform over the Brillouin zone.

For $t_1 = 1$, $t_z = 1/4$, and $\Delta = 1/2$, one has $g_{(\pi,0)} = 1$. At the two symmetry-related momenta,

$$\begin{aligned}E_{\uparrow,+}(\pi,0) &= \frac{\sqrt{5}}{2}, \qquad E_{\downarrow,+}(\pi,0) = \frac{\sqrt{13}}{2}, \\ \delta E_+(\pi,0) &= \frac{\sqrt{5} - \sqrt{13}}{2} \simeq -0.68474165,\end{aligned} \tag{23}$$

whereas $\delta E_+(0,\pi) = +0.68474165$. Figure 1 displays the momentum-space sign structure.

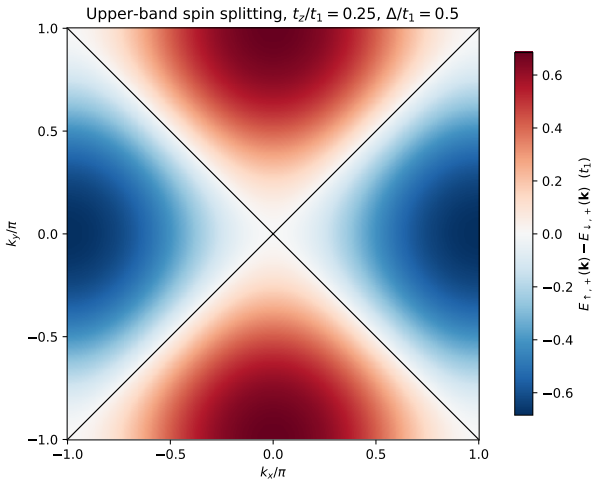


Figure 1: Upper-band spin splitting $E_{\uparrow,+}(\mathbf{k}) - E_{\downarrow,+}(\mathbf{k})$ over the Brillouin zone for $t_1 = 1$, $t_z = 0.25$, and $\Delta = 0.5$. The contrast reverses under the quarter-turn R and vanishes on the nodal lines $g_{\mathbf{k}} = 0$.

4.1 First-order Hubbard self-energy

At half filling, the combined symmetry imposes

$$n_{A\uparrow} = n_{B\downarrow} = a, \qquad n_{B\uparrow} = n_{A\downarrow} = b, \tag{24}$$

with $(a + b)/2 = 1/2$. Define the staggered moment per site by

$$m_0 = \frac{a - b}{2} = \frac{1}{2N_c}\sum_{\mathbf{k}} \frac{\Delta - g_{\mathbf{k}}}{\sqrt{t_1^2 + (g_{\mathbf{k}} - \Delta)^2}}. \tag{25}$$

The first-order onsite Hubbard self-energy is diagonal in site and spin space:

$$\Sigma^{(1)} = \frac{U}{2} I_4 - U m_0 \sigma_z \otimes \tau_z. \tag{26}$$

The first term is the half-filled chemical-potential shift. The second has the same matrix structure as the staggered exchange term and therefore renormalizes it according to

$$\Delta_{\mathrm{eff}} = \Delta + U m_0 + O(U^2). \tag{27}$$

For $t_1 = 1$, $t_z = 0.25$, and $\Delta = 0.5$, Brillouin-zone integration gives $m_0 \simeq 0.18347629$. At $U = 0.1$, this gives $\Delta_{\mathrm{eff}} \simeq 0.5183476$ and a first-order upper-band splitting of approximately $-0.70812 t_1$ at $(\pi, 0)$. The correction respects the exact covariance because it renormalizes a symmetry-invariant operator.

4.2 A finite-volume spectral stability bound

The persistence of isolated poles for sufficiently small interaction on a fixed finite lattice follows from a simple operator bound. Let $H(U) = H(0) + UV$ in a fixed particle-number sector, with $V = \sum_i n_{i\uparrow} n_{i\downarrow}$ and $\|V\| \leq N_s$, where N_s is the number of physical sites. The min–max principle bounds the displacement of each eigenvalue by $|U| N_s$. An addition

or removal energy, being a difference between eigenvalues in adjacent number sectors, can therefore move by at most $2|U|N_s$ as long as its eigenvalue branches are followed. Two initially isolated poles separated by δ_0 remain distinct under the sufficient condition

$$\delta_0 > 4|U|N_s, \tag{28}$$

provided the corresponding spectral matrix elements remain nonzero. This estimate is deliberately conservative and depends on volume; it supplies no uniform thermodynamic-limit interval.

5. Lanczos spectral benchmark on an eight-site cluster

We now test the interacting spectral structure without a Hartree decoupling. The cluster is a periodic 2×2 array of unit cells, giving four unit cells and eight physical sites. The parameters are $t_1 = 1$, $t_z = 0.25$, $t_0 = 0$, and $\Delta_{\mathrm{pin}} = 0.5$. The one-body hopping matrix reproduces equation (3), and the full onsite interaction in equation (2) is retained. At half filling, the balanced sector has $N_\uparrow = N_\downarrow = 4$ and dimension

$$\binom{8}{4}^2 = 4900. \tag{29}$$

The particle-addition and particle-removal sectors have dimension $\binom{8}{5}\binom{8}{4} = 3920$. The ground-state sector was checked across all fixed-$(N_\uparrow, N_\downarrow)$ sectors with $N_\uparrow + N_\downarrow = 8$; the lowest-energy sector is $(4, 4)$ for every reported interaction.

At zero temperature, the matrix spectral function is obtained from the canonical Lehmann representation. Writing $\mathcal{E}_m = E_m - \mu N_m$, its addition and removal contributions are

$$\begin{aligned} A_{\alpha\beta,s}(\mathbf{k},\omega) = &\sum_{m\in N+1} \langle 0|c_{\mathbf{k}\alpha s}|m\rangle \\ &\times \langle m|c^\dagger_{\mathbf{k}\beta s}|0\rangle \delta(\omega - \mathcal{E}_m + \mathcal{E}_0) \\ &+ \sum_{n\in N-1} \langle 0|c^\dagger_{\mathbf{k}\beta s}|n\rangle \\ &\times \langle n|c_{\mathbf{k}\alpha s}|0\rangle \delta(\omega + \mathcal{E}_n - \mathcal{E}_0)\,. \end{aligned} \tag{30}$$

The ground state was obtained by sparse Lanczos diagonalization. Addition and removal spectra were evaluated from this representation using 100-step Lanczos continued fractions in the $N \pm 1$ sectors. The chemical potential, independently obtained from canonical addition and removal energies, equals $\mu = U/2$ to numerical precision. Table 1 lists the dominant sublattice-traced particle-addition peaks at $(\pi, 0)$.

The spin splitting remains finite throughout the tabulated interaction range. Its magnitude grows with U in this finite cluster, although the variation of the individual peak positions is not monotonic. The dominant peak weights are also retained in the calculation. For

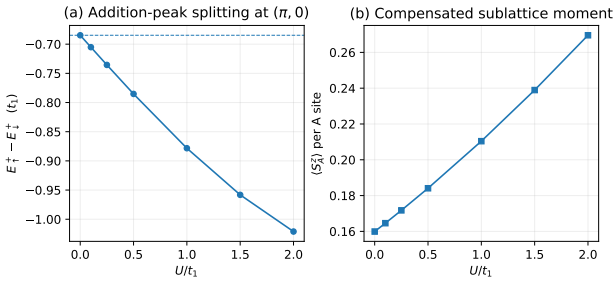


Figure 2: Lanczos exact-diagonalization results for the eight-site cluster at $\Delta_{\mathrm{pin}} = 0.5$. (a) Dominant addition-peak splitting at $(\pi, 0)$; the dashed line marks the $U = 0$ value. (b) Sublattice-A moment per site; the B-sublattice moment is equal and opposite.

$U/t_1 = (0, 0.1, 0.25, 0.5, 1, 1.5, 2)$, they are

$$\begin{aligned} W_\uparrow = (&0.72360680, 0.71758291, 0.70741048, 0.68742937, \\ &0.63631081, 0.57139656, 0.49572504), \\ W_\downarrow = (&0.91602515, 0.91703607, 0.91718415, 0.91356134, \\ &0.89048251, 0.84505792, 0.77930526). \end{aligned}$$

The peak locations at $U = 0.1$ and 0.5 are stable between 40, 60, 80, and 100 Lanczos steps; those at $U = 1$, 1.5, and 2 are stable between 80 and 100 steps. The total addition and removal spectral weights, traced over both sublattices at fixed momentum and spin, satisfy the computed anticommutator sum rules to numerical precision.

The same calculation tests the covariance at symmetry-related momenta. At $U = 0.1$, the dominant up-spin addition peak at $(\pi, 0)$ and the down-spin peak at $R(\pi, 0) = (0, \pi)$ have the same energy, 1.111037981337, and the same weight, 0.717582914734, within the Lanczos residual. At $(0, 0)$ and (π, π), where $g_{\mathbf{k}} = 0$, the spin peak energies coincide at 1.125560479. At $(\pi, 0)$ they remain distinct, as required for a nonzero momentum-resolved contrast.

The local moments obey

$$\langle S^z_A \rangle = -\langle S^z_B \rangle, \qquad M^{\mathrm{total}}_z = 0, \tag{31}$$

within numerical precision. The sublattice-A moment per site increases from 0.15990799 at $U = 0$ to 0.26956914 at $U = 2$, with the sublattice-B moment equal and opposite. The density on each site is one at the displayed precision. Figure 2 shows the interaction dependence of the peak splitting and the compensated local moment.

For comparison, the finite-cluster self-consistent Hartree equation is $\Delta_{\mathrm{eff}} = \Delta_{\mathrm{pin}} + U m_A(\Delta_{\mathrm{eff}})$. At $U/t_1 = (0.1, 0.25, 0.5, 1, 1.5, 2)$, its predicted peak splittings are

$$\begin{aligned} \delta E_{\mathrm{HF}} = (&-0.70573121, -0.73931207, -0.80139825, \\ &-0.95178123, -1.13922794, -1.34852153), \\ \delta E_{\mathrm{ED}} = (&-0.70515841, -0.73556350, -0.78526097, \\ &-0.87829369, -0.95819927, -1.02107564). \end{aligned}$$

Table 1: Dominant particle-addition peak positions at $\mathbf{k} = (\pi, 0)$ in the source-pinned eight-site Hubbard cluster. Energies are in units of t_1. The spin splitting is $E^+_\uparrow - E^+_\downarrow$.

U/t_1	$E^+_\uparrow$	$E^+_\downarrow$	$E^+_\uparrow - E^+_\downarrow$
0.00	1.11803399	1.80277564	-0.68474165
0.10	1.11103798	1.81619639	-0.70515841
0.25	1.10117148	1.83673498	-0.73556350
0.50	1.08667123	1.87193220	-0.78526097
1.00	1.06719059	1.94548428	-0.87829369
1.50	1.06549092	2.02369019	-0.95819927
2.00	1.08850146	2.10957710	-1.02107564

The difference grows with interaction, showing that a static Hartree description increasingly overestimates the splitting in this cluster. The exact diagonalization therefore supplies a nonperturbative finite-system check that the spectral contrast survives onsite interactions and remains compatible with zero net magnetization.

6. Nonlocal second-order dynamical self-energy

The finite-cluster calculation establishes the spectral structure at selected interactions. To resolve the frequency dependence of interaction effects, we separately evaluate the bare-propagator expansion through second order in U for the symmetry-pinned two-sublattice model. This calculation uses $t_1 = 1$, $t_z = 0.25$, $\Delta_{\mathrm{pin}} = 0.5$, $t_0 = 0$, $U = 0.1$, and $\beta = 100$ for the low-temperature real-axis estimates.

For physical sites i, j, the complete second-order self-energy in imaginary time is

$$\Sigma^{(2)}_{ij,s}(\tau) = -U^2 G^0_{ij,s}(\tau) G^0_{ij,\bar{s}}(\tau) G^0_{ji,\bar{s}}(-\tau). \tag{32}$$

Although the interaction is onsite, the second-order self-energy is nonlocal in space: no restriction $i = j$ is imposed. Here G^0 is the exact matrix propagator of the pinned noninteracting two-sublattice Hamiltonian. Define the real-space spectral matrix

$$A^0_{ij,s}(\epsilon) = -\frac{1}{\pi} \operatorname{Im} G^{0,R}_{ij,s}(\epsilon). \tag{33}$$

The retarded self-energy can be written, for $\operatorname{Im} z > 0$, as

$$\Sigma^{(2),R}_{ij,s}(z) = U^2 \int \mathrm{d}\epsilon_1\, \mathrm{d}\epsilon_2\, \mathrm{d}\epsilon_3\, A^0_{ij,s}(\epsilon_1) A^0_{ij,\bar{s}}(\epsilon_2) A^0_{ji,\bar{s}}(\epsilon_3) \times \frac{(1-f_1)(1-f_2)f_3 + f_1 f_2 (1-f_3)}{z - \epsilon_1 - \epsilon_2 + \epsilon_3}, \tag{34}$$

where $f_i = f(\epsilon_i)$. The products in the integrand are the indicated real-space matrix elements. Fourier transformation in the cell separation yields $\Sigma^{(2)}_{ab,s}(\mathbf{k}, z)$.

6.1 Numerical checks

Equation (34) is the standard three-line spectral form of the second-order Hubbard self-energy; its diagrammatic origin and Matsubara formulation are reviewed in Refs. [4, 5]. The spectral convolution was compared against direct imaginary-time evaluation at $N_k = 12 \times 12$, $\beta = 12$, 192 midpoint imaginary-time samples, and energy spacing $\delta\epsilon = 0.005$. At $z = i\pi/\beta$, the maximum absolute discrepancy was 8.86×10^{-7}, corresponding to a relative discrepancy of 2.01×10^{-3}. This difference is consistent with the finite energy- and time-grid discretizations and checks the frequency combination and overall sign in equation (34).

The computed self-energy obeys the combined-symmetry relation

$$\Sigma^{(2),R}_{\uparrow}(\mathbf{k}, z) = \tau_x \Sigma^{(2),R}_{\downarrow}(R\mathbf{k}, z) \tau_x. \tag{35}$$

Across the tested real frequencies and the full 12×12 momentum grid, the maximum covariance residual is 1.35×10^{-18}. Defining the Hermitian imaginary part by

$$\operatorname{Im}_H \Sigma = \frac{\Sigma - \Sigma^\dagger}{2i}, \tag{36}$$

we find $\operatorname{Im}_H \Sigma^R \preceq 0$ on the tested grid with a finite positive regulator, as required by retarded causality. The small negative values below the decay threshold scale with the regulator and are not interpreted as physical linewidths.

6.2 On-shell pole correction

At $\mathbf{k} = (\pi, 0)$, $g_{\mathbf{k}} = 1$. The bare upper-band energies are

$$E^0_{\uparrow,+} = \frac{\sqrt{5}}{2} = 1.118033989, \qquad E^0_{\downarrow,+} = \frac{\sqrt{13}}{2} = 1.802775638. \tag{37}$$

At $\beta = 100$, the bare densities are $n_{A\uparrow} = n_{B\downarrow} = 0.683476290$ and $n_{B\uparrow} = n_{A\downarrow} = 0.316523710$, giving $m_0 = 0.183476290$. After subtracting the common half-filled Hartree shift $U/2$, the first-order matrix is $-sUm_0\tau_z$.

The strict second-order pole correction includes the diagonal Hartree expectation, the on-shell projection of $\operatorname{Re} \Sigma^{(2),R}$,

Table 2: On-shell upper-band pole corrections at $(\pi, 0)$ through order U^2 for $U = 0.1$. Energies are in units of t_1.

Contribution	↑	↓
Bare pole	1.118033989	1.802775638
Hartree shift	-0.008205309	+0.015266150
$\mathrm{Re}\,\Sigma^{(2)}$ projection	+0.000339373	-0.000324133
Interband mixing	+0.000120438	+0.000028728
Total shift	-0.007745497	+0.014970745
Corrected pole	1.110288491	1.817746383

and the second-order interband mixing induced by the first-order Hartree matrix. For an upper-band eigenvector $|u_{s,+}\rangle$, the latter is

$$\delta E^{(2)}_{\mathrm{mix}} = \frac{|\langle u_{s,-}|\Sigma^{(1)}_H|u_{s,+}\rangle|^2}{E^0_{s,+} - E^0_{s,-}}. \tag{38}$$

The common order-U^2 chemical-potential countershift at fixed density moves both spin poles equally and does not affect their difference. The numerical decomposition is given in table 2.

The corrected splitting is

$$\delta E^{(O(U^2))}_{\mathrm{pole}} = -0.707457891, \tag{39}$$

compared with the bare value -0.684741649. The change separates into a Hartree contribution -0.023471459, a dynamical second-order contribution $+0.000663507$, and an interband-mixing contribution $+0.000091710$. Their sum is -0.022716242. This is an asymptotic weak-coupling result, not a finite-U solution of the pole equation.

6.3 Zero-temperature decay threshold

For the pinned benchmark, both spin sectors have a minimum positive excitation energy $E_{\mathrm{min}} = t_1 = 1$. At zero temperature, the particle-decay part of the second-order convolution has support only when

$$\omega = \epsilon_1 + \epsilon_2 - \epsilon_3 \geq E_{\mathrm{min},\uparrow} + E_{\mathrm{min},\bar{s}} + E_{\mathrm{min},\bar{s}} = 3t_1. \tag{40}$$

The hole part has support only for $\omega \leq -3t_1$. Thus

$$\mathrm{Im}\,\Sigma^{(2),R}_s(\omega) = 0 \quad \text{for} \quad |\omega| < 3t_1, \qquad T = 0. \tag{41}$$

The two upper poles at $1.118t_1$ and $1.803t_1$ lie below this threshold and have no intrinsic order-U^2 linewidth at zero temperature in this insulating model. At $\beta = 100$ and regulator $\eta = 0.001$, the projected residual imaginary parts are approximately -1.25×10^{-7} and -3.67×10^{-7} for the two spins; their scaling with η identifies them as regulator tails. Thermally activated channels at finite temperature are not included in the zero-temperature threshold statement.

7. Discussion and conclusion

The combined symmetry provides an exact many-body relation between opposite-spin spectral matrices at momenta related by a quarter-turn. Its immediate consequence is not a universal finite splitting at every momentum, but a precise sign reversal of the spin-resolved spectral contrast and the cancellation of its Brillouin-zone integral. The two-sublattice Hubbard model realizes the relation explicitly: the staggered source is invariant under the combined operation, while the anisotropic hopping form factor changes sign under the spatial rotation. The spectrum therefore admits a momentum-dependent spin splitting without a uniform spin polarization.

The interaction calculations show two distinct aspects of this statement. First, the Hartree term renormalizes the symmetry-allowed staggered exchange, and an eight-site Lanczos calculation finds that the dominant spin-resolved addition peaks remain separated across the reported values of U. Second, the full nonlocal second-order self-energy preserves the same matrix covariance to numerical precision. Its real-frequency contribution changes the two on-shell poles differently, while the zero-temperature spectral support places those poles below the lowest second-order decay threshold. The exact covariance is thus compatible with a frequency-dependent and nonlocal self-energy; it is not an artifact of a static band description.

The finite-cluster calculation uses a nonzero staggered source, $\Delta_{\mathrm{pin}} = 0.5$. The combined symmetry remains exact in this source-pinned state and enforces zero net magnetization. The result should therefore be read as an interacting spectral realization of the altermagnetic symmetry pattern in a compensated domain. It does not determine whether the zero-source electron model spontaneously selects that domain in the thermodynamic limit. That question requires a separate treatment of competing ordering channels and finite-size scaling; it is not needed for the Green-function covariance theorem established here.

The central conclusion is that the relation between momentum-resolved spin splitting and zero uniform magnetization can be formulated directly at the level of the exact interacting Green function. This formulation supplies a symmetry constraint for diagrammatic approximations, numerical self-energies, and spectral calculations: each approximation that respects the combined symmetry must preserve equation (13) and equation (35). The two-sublattice Hubbard results provide an explicit interacting benchmark for that constraint.

References

[1] L. Šmejkal, J. Sinova, and T. Jungwirth, Phys. Rev. X **12**, 031042 (2022). doi:10.1103/PhysRevX.12.031042.

[2] L. Šmejkal, J. Sinova, and T. Jungwirth, Phys. Rev. X **12**, 040501 (2022). doi:10.1103/PhysRevX.12.040501.

[3] S.-W. Cheong and F.-T. Huang, npj Quantum Mater. **10**, 38 (2025). doi:10.1038/s41535-025-00756-5.

[4] G. Bulk and R. J. Jelitto, Phys. Rev. B **41**, 413 (1990). doi:10.1103/PhysRevB.41.413.

[5] A. L. Fetter and J. D. Walecka, *Quantum Theory of Many-Particle Systems* (McGraw-Hill, New York, 1971).